April 2013

In-Vivo Like Studies of the hIAPP Amyloid Precursors by DRS

Yusuke Hirai
Worcester Polytechnic Institute

In-vivo Like Studies of the h-IAPP Amyloid Precursors Using Dielectric Relaxation Spectroscopy

A Major Qualifying Project Report
Submitted to the Faculty of the
WORCESTER POLYTECHNIC INSTITUTE
in partial fulfillment of the requirements for the
Degree of Bachelor of Science
in
Physics
By
Yusuke Hirai
April, 2013

APPROVED:

_____

Prof. Izabela R. Stroe
Physics
Project Advisor

Abstract

Amyloidosis is a pathological condition that refers to a number of diseases characterized by the formation of insoluble amyloid deposits in tissues and organs, such as liver, spleen, kidneys, and brain.[1] The deposits are caused by the misfolding and aggregation of amyloidogenic peptides into organized, fibrillar structures. Examples of the most common amyloid-related diseases are Alzheimer's disease, Type II diabetes, Huntington's disease, Parkinson's disease, Creutzfeldt-Jakob disease, and even transmissible diseases, such as spongiform encephalopathies.[2] An emergent theory establishes that fibrils may not be the toxic form of amyloidogenic structures, but rather small oligomers and protofibrils are now believed to be the primary source for damage to cellular function.

In this research, we study amyloidogenic proteins that trigger Type II diabetic disease. Recent studies has shown that early detection of Type II diabetic disease may prevent and/or slow the progression of the debilitating long term complications of the disease. It is known that amyloid formation in Type II diabetic disease involves aggregation of monomers of human islet amyloid polypeptide (h-IAPP) into oligomers, protofibrils, and fibrils. Therefore, early detection of this disease involves detection of the toxic forms such as oligomers, protofibrils, and fibrils of the h-IAPP.

We propose Dielectric Relaxation Spectroscopy (DRS) as an early detecting measurement tool to test the sensitivity of DRS. We measure the dielectric response of amyloidogenic h-IAPP and non-amyloidogenic r-IAPP as a function of frequency ($f = 10^{-3} - 10^{7} Hz$), temperature (193K to

283K), and incubation time (0-120 h). To mimic in-vivo like conditions, the proteins are measured in bovine serum albumin. We first looked at permittivity as a function of frequency and compared the differences between h-IAPP and r-IAPP. We used two Havrilik-Negami functions plus conductivity to fit the α- and β-relaxation processes then we determined the relaxation time for both processes and calculated the corresponding activation energies. The relaxation time was plotted as a function of inverse temperature which then used for determining the activation energy. The dielectric strength was also determined to observe structural changes in the processes.

Index

1. Introduction

1.1 Diabetic Disease

According to American Diabetes Association and World Health Organization, 25.8million children and adults in the United States--8.3% of the population—and 347 million people in the world have diabetes. Diabetes is a disease in which the blood glucose, or sugar, levels are too high. Glucose comes from the foods eaten. Insulin is a hormone that helps the glucose gets into cells to give them energy. There are Type I and Type II diabetes. With type I diabetes, the body does not make insulin. This can be caused by genetics, environment, vires, diet, and chemical and drugs. With type II diabetes, the more common type, the body does not make or use insulin well. Without enough insulin, the glucose stays in blood.

Diabetes is the leading cause of kidney failure, nontraumatic lower-limb amputations, and new cases of blindness among adults in the United States. It is also one of the major causes of heart disease and stroke. According to recent statistics, Type II diabetic disease is the seventh leading cause of death in the United States.[3]

Direct medical costs for diabetic disease are estimated at $116 billion in 2010. This is almost double the amount of medical expenses for cancer. Average medical expenditures among people with diagnosed diabetes were 2.3 times higher than what expenditures would be in the absence of diabetes. Indirect costs such as disability, work loss, premature mortality are estimated at

$58 billion. Recent studies indicate that the early detection of diabetes symptoms and treatment can decrease the chance of developing the complications of diabetes.[3]

Amyloid deposits of human Islet Amyloid Polypeptide (IAPP) or amylin have been found post-mortem in the pancreatic β-cells of more than 90% of patients with Type II diabetes. Amylin is co-secreted with insulin by the pancreatic β-cells in the islets of Langerhans as a regulator of glucose uptake and gastric emptying.[4] The 37 residue polypeptide amylin is soluble and non-toxic in its natural form.[5] Environmental conditions and genetic predisposition cause amylin to aggregate and form toxic amyloid fibrils. The amyloid deposits cause death of the pancreaticβ-cells leading to reduced production of insulin and eventually Type II diabetes.[6] Basal amylin serum concentration is abnormal in patients with Type II diabetes and thus, novel detection of amylin in blood serum is a central focus of our studies.

1.2 IAPP

Islet amyloid polypeptide (IAPP or Amylin) is a 37 amino-acid, β-cell peptide which is co-stored and co-released with insulin. IAPP is derived from a larger precursor peptide, proIAPP, (67amino acids in man) and proteolyticallt cleaved at the N- and C- terminal junctions by prohomone converses 1/3 and2 within the β-cell secretory granule as the granule matures.[7] IAPP has been found to be amyloidogenic in humans, monkeys, and cats but not amyloidogenic in hamsters, mice, and rats. The variations in amino acid sequences between species point to a theory that specific hydrophobic

regions are responsible for amyloid formation. For example, in human IAPP, sequence 20-29 has been shown in vivo as a source for amyloid fibril formation.

Recent theory suggests that cell membrane toxicity by IAPP is caused by pore-like disruption by oligomer and protofibril species.[8] The oligomers form ion channels in the lipid bilayers on the pancreatic β-cell membrane. These small pores allow cell contents to pass through, causing destabilization and cell death.[9] A cascading effect then follows where amylin aggregation destroys β-cells leading to decreased insulin. The remaining β-cells try to compensate by releasing more insulin and thus, more amylin which leads to further destruction of β-cells.[10]

Synthetic h-IAPP in buffer solutions is rapidly converted to β-sheet and fibrils. In the secretory granule, IAPP is at a high concentration; this is approximately 4mmol/l based in a ratio if 1:10 with insulin in pancreatic extracts and an estimated concentration of granular insulin of 40 mmol/l; at this concentration, synthetic h-IAPP would be rapidly converted into fibrils. This suggests that the peptide must be stabilized to prevent oligomerisation and fibril formation in vivo. Many laboratories show that insulin will inhibit IAPP fibril formation in vitro; IAPP and insulin form heteromolecular complexes in vitro suggesting that insulin stabilizes to IPAA or have a stabilizing effect and, therefore, any process that results in inefficient proinsulin processing could affect IAPP fibril formation in Type II diabetic disease.

1.3 Protein Folding and Aggregation

In aqueous environments, proteins cluster to form tightly-packed structures with non-polar cores. The ordering of solvent, known as the hydrophobic effect, is an important driving force in protein folding and aggregation. The hydrophobic effect is a process in which non-polar groups cluster in order to minimize surface interactions with water. Amphiphilic molecules, consisting of strongly polar and non-polar groups exhibit this behavior. Amphiphilic molecules characteristically form micelles in which the non-polar ends combine to form a hydrophobic domain of hydrocarbon tails while polar ends form ionic interactions with the solvent (Figure 1).[1 1]

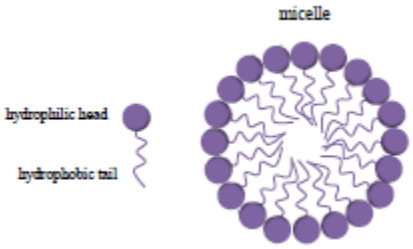

Figure 1: Hydrophobic tails bury in the interior during micelle formation as hydrophilic regions interact with polar solvents.

When a protein is placed in water, the hydration layer is disturbed. The water competes with the hydrogen bonding in the hydrophobic domain of the protein causing a reordering of the bound water. The bound water is then released and the hydrophobic regions begin to cluster. This is driven by a thermodynamically favorable event where the movement of bound, ordered water moves to free,

bulk-like water in the direction of increased entropy. When a protein folds, the hydrophobic and hydrophilic regions combine via non-covalent interactions to form secondary structures, such as α-helices and β-sheets. The α-helix is formed by hydrogen bonds between NH and CO groups of the main chain. The β-sheet conformation is formed by either parallel or anti-parallel stacking between polypeptide strands (Figure 2).

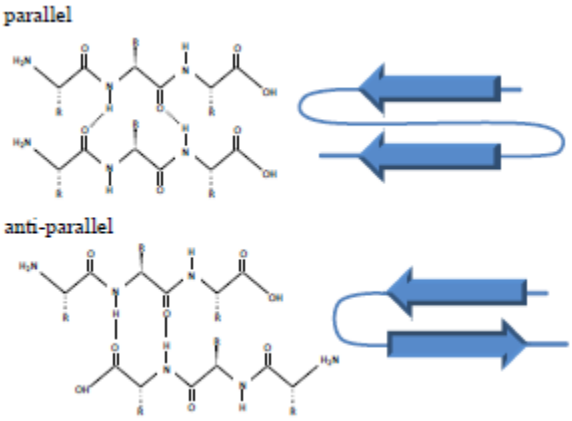

Figure 2: Picture of parallel and anti-parallel stacking of protein. [11]

1.4 Biological Water

Biological water at the interface of proteins is critical to their equilibrium structures and enzyme function and to phenomena such as molecular recognition and protein–protein interactions. The picture below (Figure 3) is a hydration map of amyloidogenic protein. There are four categories of water surrounding the protein: Bulk water which does not interact with the surface of the protein, highly structured water which intimately interacts with the surface of the protein, caged water which

is trapped in between the cells when proteins aggregate, bulk-like water which exists due to structural defects. These properties are very important in the measurement of dielectric spectroscopy. Our hypothesis is that these water structure changes during aggregation process. It is important to note that the observed relaxation processes do not originate in the protein itself, but in the bulk solvent and the hydration shell.[1 2]

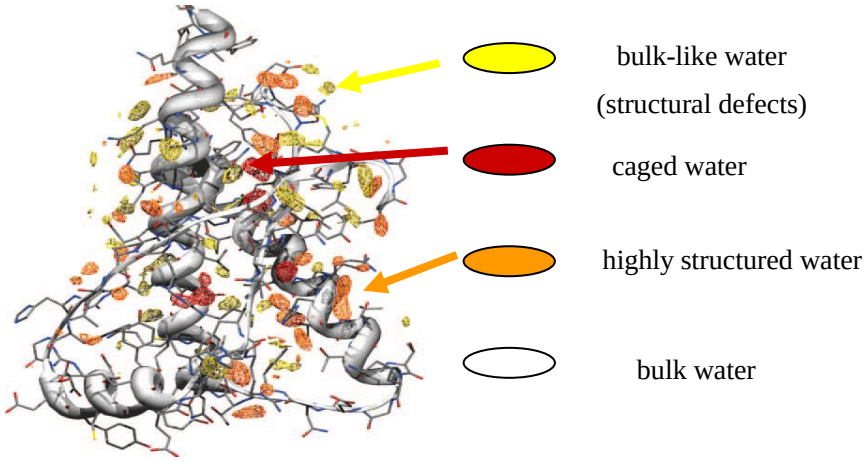

Figure 3: Hydration map of amyloidogenic protein. (De Simone et al., *PNAS*, 2005)

2. Dielectric Relaxation Spectroscopy as a Tool for Studying Amyloidgenic Peptide

2.1 Polarization Mechanism

We observe a number of polarization mechanisms in dielectric relaxation over a broadband of frequencies: Electron polarization, Atomic polarization, Orientation polarization, Ionic polarization, Electrode polarization. These polarizations are summarized below.[1 3]

Electron polarization is the deformation of the atomic electrons in the presence of an electric field. This process occurs at high (optical) frequencies, near 10^{15} Hz.

Atomic polarization is the displacement of atoms or groups of atoms relative to one another within a molecule in the presence of an electric field. This process occurs at high (microwave to optical) frequencies, at approximately 10^{12} - 10^{14} Hz.

Orientation polarization, also known as dipole relaxation, is the rotation and orientation of a molecule in the presence of an electric field. Only polar molecules with permanent dipole moments will exhibit orientation polarization. This rotation is impeded by thermal motion and viscosity and this, the relaxation time is highly dependent on the frequency of the applied electric field, temperature, and pressure. The frequency range is typically in the radio frequencies (MHz) and below.

Ionic polarization is the displacement of positive ions in the direction of an applied electric field with negative electrons in the opposing direction in an ionic lattice. The result is a net dipole

moment to the entire structure. Ionic polarization is predominately at very low (DC) frequencies and only has a weak temperature dependence. Commonly referred to as DC conductivity, it only presents dielectric losses to the system.

Electrode polarization is an impedance of the mobility of charge carriers at the interface of ionic materials and a metal conductor.[14] Electrode polarization may introduce a large dielectric response at low frequencies.

2.2 Our Approach and Set up

Our approach is to detect amyloid precursors using Dielectric Relaxation Spectroscopy (DRS). Detection is based on assessing the Dielectric Relaxation signal of water surrounding preamyloid oligomers and fibrils.

DRS is an effective technique suitable for the study and characterization of biological materials and systems. Water structure near the surfaces of proteins is subject to hydrogen bonding of water molecules to proteins and electrostatic interaction due to the large dipole moment.[15,16] Studies of relaxation processes give us insight into structural and dynamical properties of biomaterials. More specifically, our assumption is that when there is a change in the form of the water surrounding proteins, a shift in the dielectric spectra is observed.

The picture below (Figure 4) shows the DRS system we used (4.a), the sample holder (4.b), and the sample cell (4c). Liquid nitrogen is used to cool down the sample when measurement is in

process. The system is capable of cooling the sample as low as 80 K and as high as 400 K. Also, it can span frequencies of $f = 10^{-3} - 10^{7} Hz$. This particular cell is advantageous when analyzing dielectric spectra of liquids at subfreezing temperatures. The design is such that the cell does not need to be completely full and thus reduces the effects of thermal expansion and fluid leakage.[17] This geometry keeps the same amount of fluid between the capacitive plates over a wide range of temperature.

Figure 4: Dielectric relaxation spectroscopy (a), sample holder (b), and sample cell (c).

The basic of the measurement is shown in Figure 5. After setting the sample in the sample cell and placing it on the sample holder, a sinusoidal voltage is applied and the current is measured. When the voltage is applied to a dielectric sample, the dipoles will align and current is induced. The ratio of the voltage to current is the impedance which is inverse proportional to the dielectric permittivity of the sample. The relationship between the complex dielectric permittivity and the

measured impedance is given by Eq. 1.

$$\boldsymbol{\varepsilon^* = \varepsilon' - i\varepsilon'' = \frac{1}{i\omega C_0 Z(\varepsilon)^*}} \qquad (1)$$

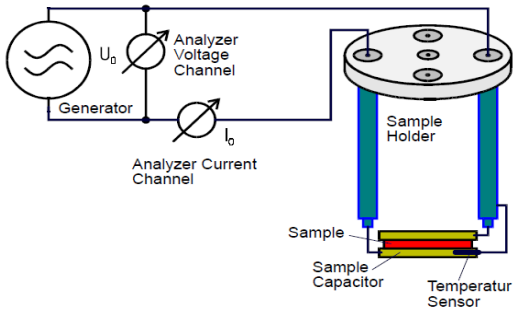

Figure 5: Schematic picture of the experimental set-up.

2.3 Data Analysis from Permittivity

In the measurements, it is reasonable to consider that at t=0h the state of the proteins are misfolded monomers then at t=24h dimers, at t=48h oligomers and at t=120h amyloid deposits. A typical data of the imaginary part of permittivity is shown in figure 6 (a). This behavior is understood by the structure of the water surrounding the protein as shown in figure 6 (b). As the protein aggregates with another protein, the highly structured water liberate to bulk water, which leads to decrease in the spectra. Therefore as it aggregates more and more, we see that the magnitude of the spectra decreases.

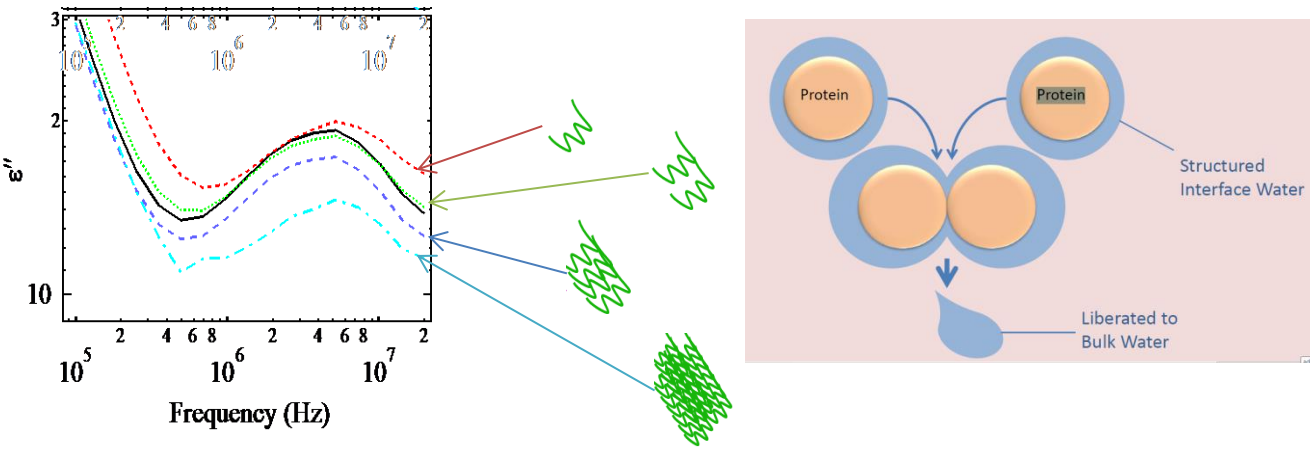

Figure 6: Typical graph of imaginary permittivity vs. frequency (a) and simplified aggregation process at the water structure level (b).

2.4 Curve Fitting and Data Analysis

Curve fitting of the dielectric permittivity data was done in the frequency domain using the WinFIT program. The fitting procedure begins with a visual estimate of the conductivity, τ, and Δε parameters. There are three relaxation processes: α-relaxation, β-relaxation, and conductivity (σ). Equations that are used for these processes are: for α-relaxation;

$$\boldsymbol{\varepsilon(\omega) = \varepsilon_\infty + \frac{\varepsilon}{(1+\omega\tau)^\gamma}} \quad , \quad (2)$$

for β-relaxation;

$$\boldsymbol{\varepsilon(\omega) = \varepsilon_\infty + \frac{\varepsilon}{1+\omega\tau}} \quad , \quad (3)$$

and for conductivity;

$$\boldsymbol{\delta(\omega) = -i(\frac{\delta_0}{\varepsilon_0 \omega})^N.} \qquad (4)$$

The f_{max} and the $\boldsymbol{\tau_{max}}$ is related by;

$$\boldsymbol{f_{max} = \frac{1}{2\pi\tau_{max}}.} \qquad (5)$$

Furthermore, the activation energies can be modeled by utilizing the fits to the permittivity data over a broad range of temperatures. The activation energy is calculated by using Eq.6;

$$\boldsymbol{\tau = \tau_0 e^{-E_a/K_B T}.} \qquad (6)$$

3. Studies of the h-IAPP and the r-IAPP in DI H_2O Buffer

3.1 Overview

Protein association and aggregation causes a redistribution of biological water molecules at the protein-water interface.[18] Studies show that amyloidogenic aggregates are characterized by an increased number of poorly dehydrated hydrogen backbones and large surface densities of patches of bulk like water which favor protein association.[19] The water dynamics in the vicinity of the amyloidogenic aggregates is different than the monomeric form and thus there is a decrease of patches which are occupied by molecules with bulk-like water behavior (i.e. no translations or rotations). The change on the surface depends on how many patches of structural defects remain after the formation of dimers, tetramers, oligomers, and protofibrils.[20] We hypothesize that this change in the long-lived water structures provides the change in the dielectric relaxation signal of the structure. Our theoretical model suggests that measurement over a wide range of frequencies produces a differentiated signal for the different configurations of protein-water interface.

In this chapter, dielectric spectroscopy data and analysis is presented for an amyloidogenic peptide and its non-amyloidogenic analog. Amyloidogenic peptide human islet amyloid polypeptide, h-IAPP (22-27) was used as a model for studying protein aggregation and beta sheet formation in a deionized water buffer. Its non-amyloidogenic analog, rat islet amyloid polypeptide, r-IAPP (20-29) was selected as a control material. Trends of dielectric spectra as a function of incubation time and temperature are explored within.

3.2 Sample Preparation

Lyophilized peptides were obtained from AnaSpec, Inc in quantities of 0.5 mg and 1.0 mg. The vials were stored at approximately -20 ℃ until the time of reconstitution. Deionized water, 18.2 MΩcm minimum, was used to dilute and rehydrate the peptides to a concentration of approximately 100 μM and stored in a sterile vial. The samples were then mixed by repeated inversion of the vials and set to incubate for 0, 8, 24, 48, and 120 hours at room temperature. A separate sample was prepared for each time point. Glycerol, 99% minimum from Sigma was then added to a final concentration of 50 μM peptide in 50%-50% by weight DI H2O-glycerol solvent. The samples were again mixed by repeated inversion of the vials. The samples were then placed in the Novocontrol BDS 1307 stainless steel sample cell.

3.3 DRS Measurement

Data were collected using the Novocontrol Alpha-A Analyzer and Quatro Cryosystem in gain phase measurement mode with an AC probing voltage of 1.000 V_{RMS}. A liquid nitrogen cryostat was used to control temperature from 283 K down to 133 K at 5 K intervals. We selected 60 data points in a frequency range from$10^{-3} - 10^{7} Hz$, spaced evenly in a logarithmic scale. Data for each temperature point was collected in duplicate to ensure temperature stabilization and mitigate thermal hysteresis. The second, temperature stabilized duplicates were used for analysis.

3.4 Results and Discussion

3.4.1 Permittivity vs. Frequency

Figure 8- 11 show permittivity data for h-IAPP and r-IAPP as a function of frequency at different incubation times with the solvent at temperatures 223 K, 213 K, 203 K, 193 K, 183 K, 173 K, 163 K, and 153 K. The magnitude of the dielectric loss peaks of the h-IAPP follows a different trend than the r-IAPP. At temperature 203 K and 193K, there is no significant behavior in the conductivity for the h-IAPP but increase conductivity occurs in the r-IAPP. Also, at temperature 183 K and 173 K, there is a consistent shift by time in conductivity for r-IAPP at 183K. This is not observed with h-IAPP. Moreover, at 163 K and153 K, the peaks of the β-processes for r-IAPP shift to higher magnitude over time. The shift of the β-process for h-IAPP at 153K is almost opposite to this behavior.

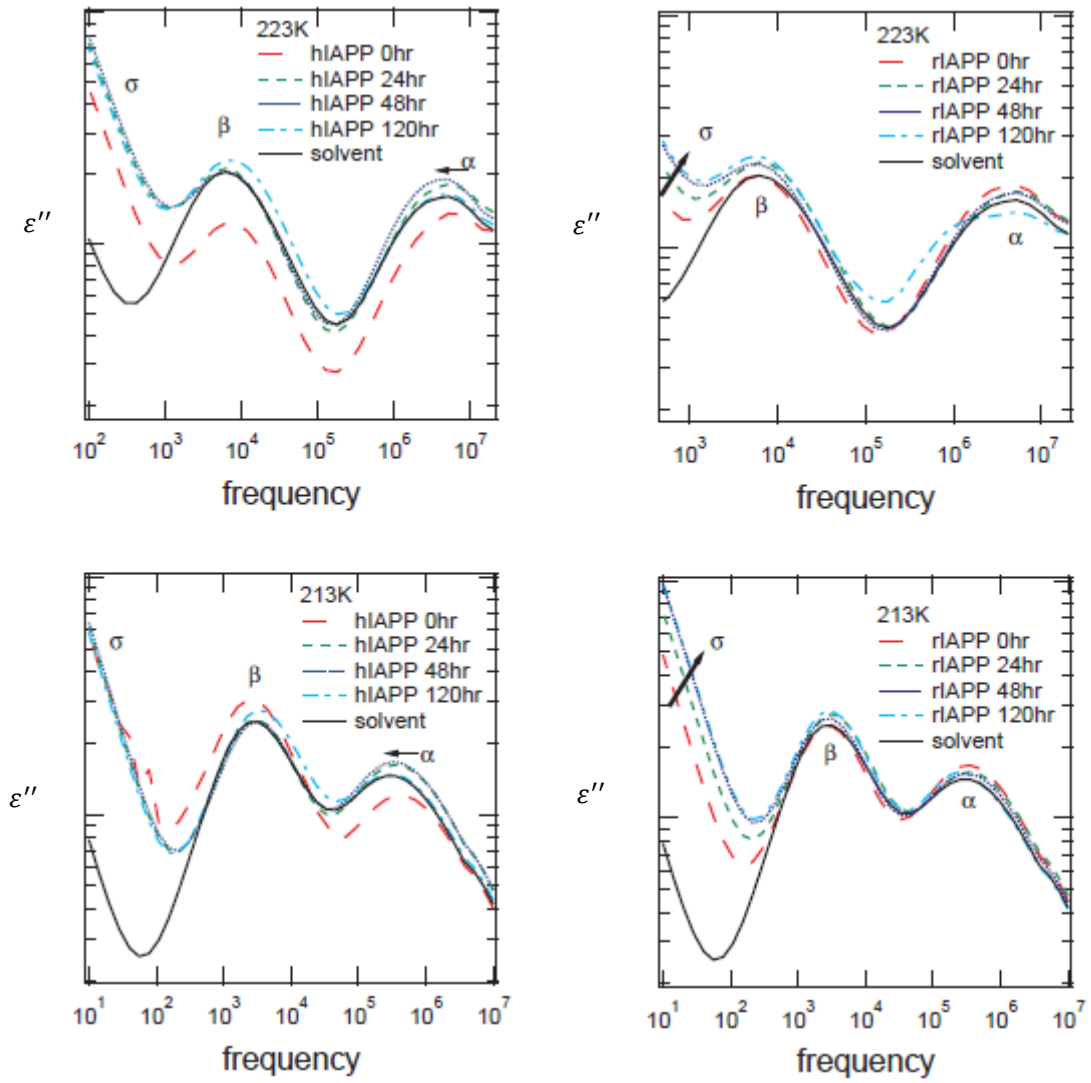

Figure 7: Dielectric loss ε'' as a function of frequency for h-IAPP and r-IAPP at temperatures 223K and 213K and incubation periods of 0, 24, 48, and120 hours. The arrows in the h-IAPP depict shifts of the α-process to slightly lower frequency, but there is no consistent change in conductivity and β-process. The arrows on r-IAPP show the trend of the increasing conductivity over time, which are not seen in h-IAPP. Change in β-process is due to the result of the change in conductivity and not a process change.

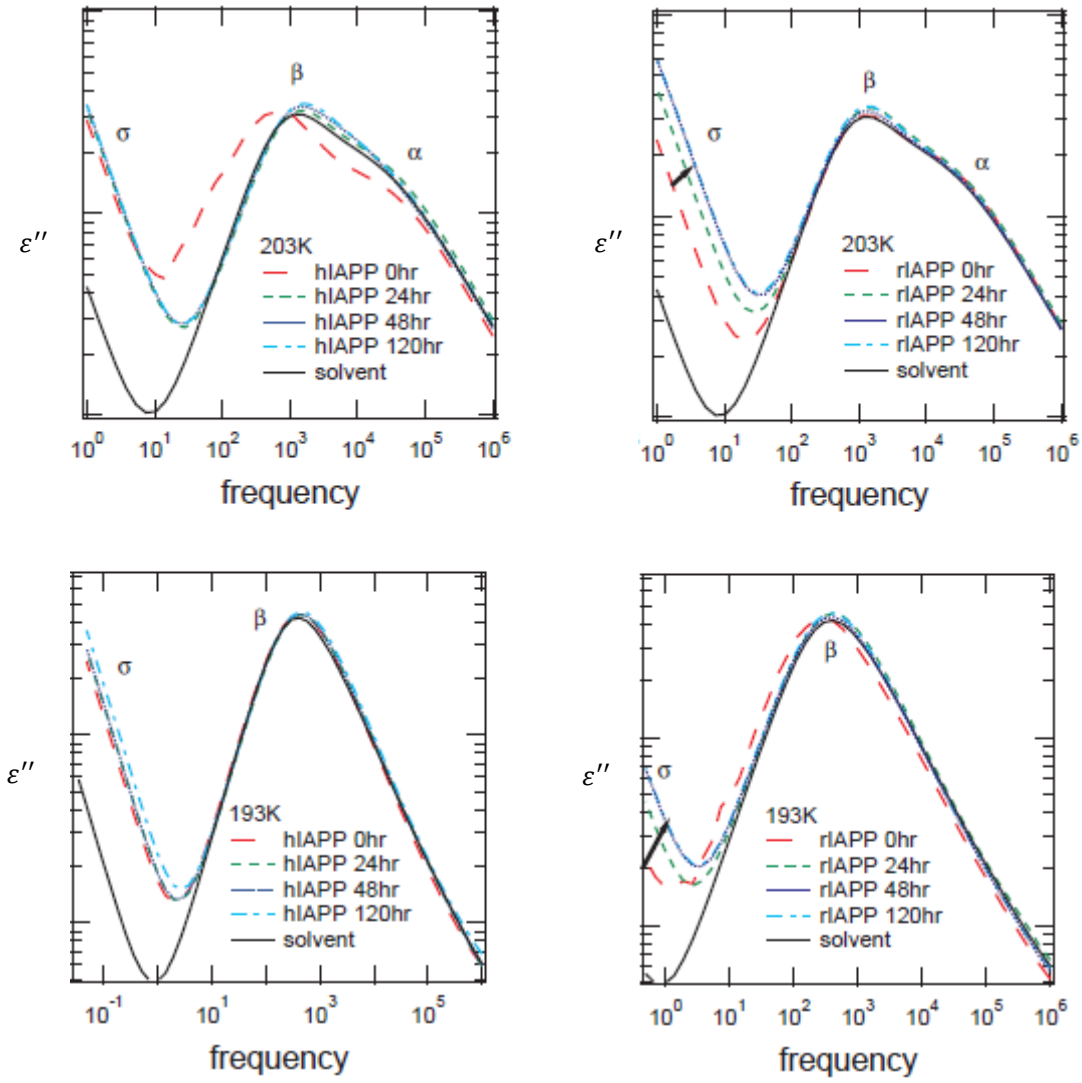

Figure 8: Dielectric loss ε'' as a function of frequency for h-IAPP and r-IAPP at temperatures 203K and 193K and incubation periods of 0, 24, 48, and120 hours. Both for the h-IAPP and the r-IAPP, α-process shifted towards β-process as the temperature lowers. There is no significant behavior in the conductivity for the h-IAPP but increase conductivity occurs in the r-IAPP.

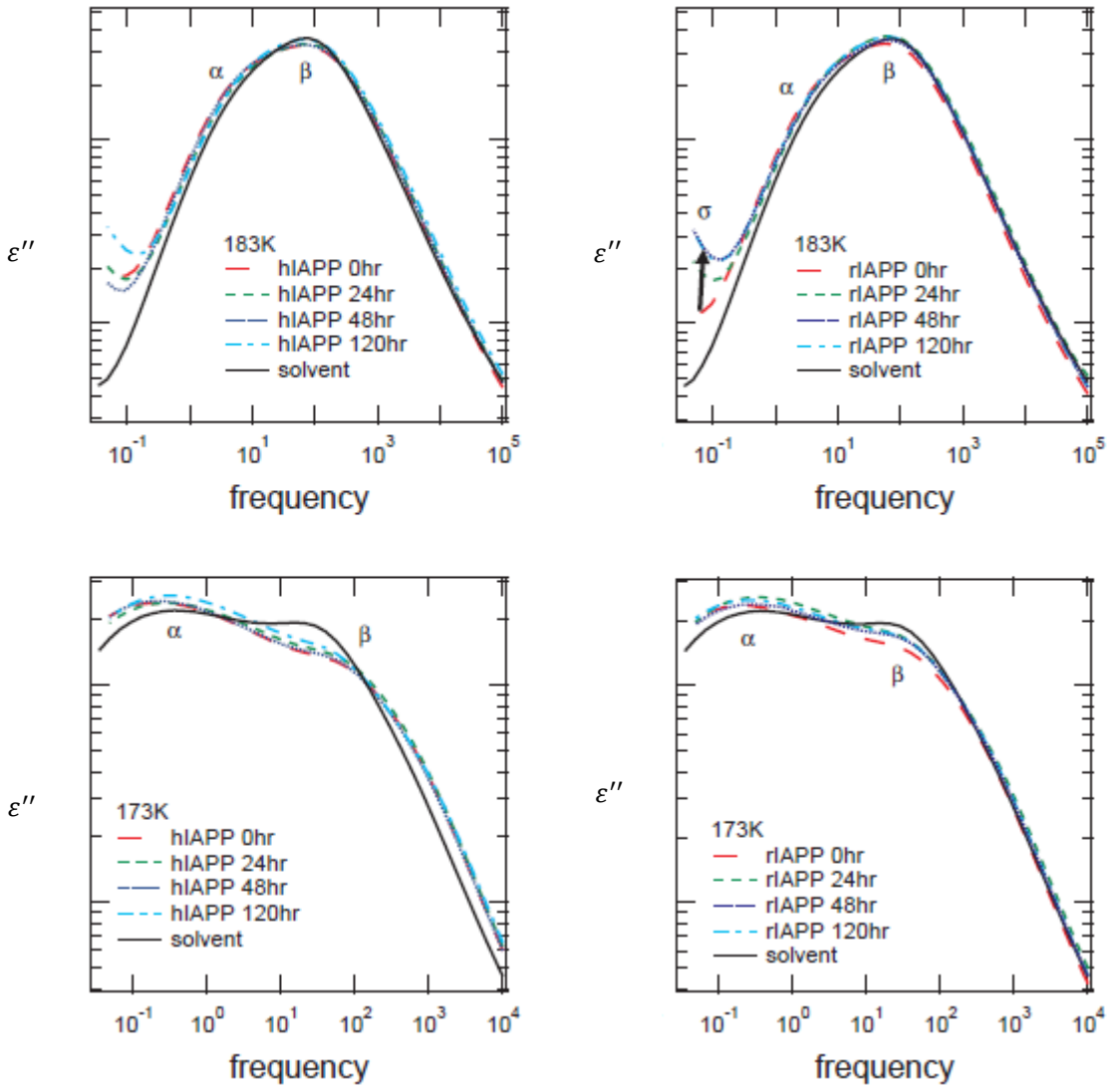

Figure 9: Dielectric loss ε'' as a function of frequency for h-IAPP and r-IAPP at temperatures 183K and 173K and incubation periods of 0, 24, 48, and120 hours. The α-process shifts to even lower frequency than the β-process. There is a consistent shift by time in conductivity for r-IAPP at 183K. This is not observed with h-IAPP.

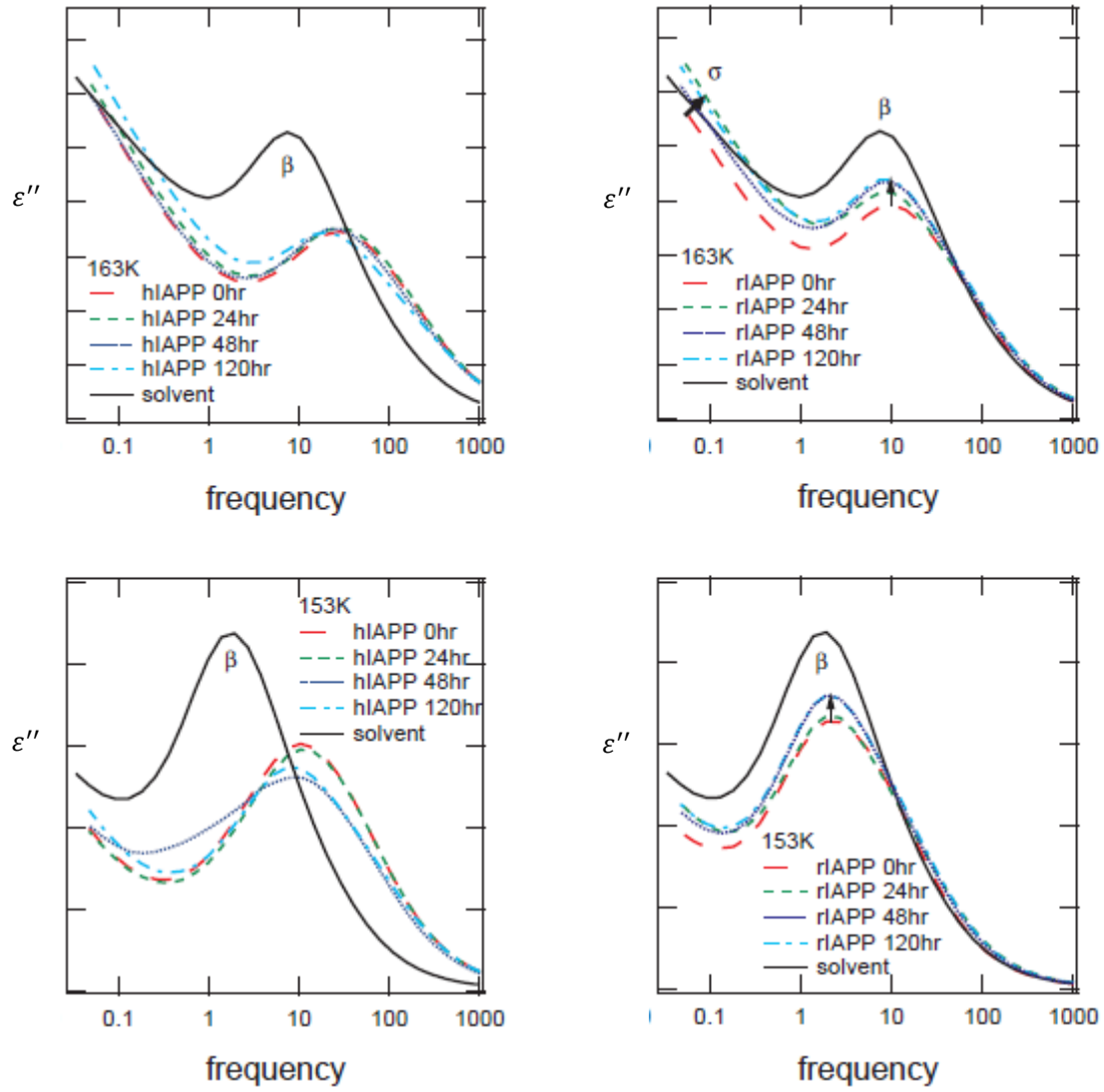

Figure 10: Dielectric loss $\boldsymbol{\varepsilon''}$ as a function of frequency for h-IAPP and r-IAPP at temperatures 163K and 153K and incubation periods of 0, 24, 48, and120 hours. Only β-processes are observed in this temperature rage except for r-IAPP at 163K where conductivity is observed. The peaks of the β-processes for r-IAPP shift to higher magnitude over time. The shift of the β-process for h-IAPP at 153K is almost opposite to this behavior.

3.4.2 Relaxation time vs. 1000/T

By using our fitting functions, the maximum frequency (f_{max}) of the imaginary part of the permittivity of α- and β-relaxation processes were determined. The maximum frequencies were plotted as a function of inverse temperature these are known as Arrhenius plot (Figure 12-14). The β-relaxation process follows a linear, or Arrhenius behavior throughout the temperature range. The α-relaxation process follows a slight non-linear Vogel-Fulcher-Tammann (VFT)-type behavior that is expected in glassforming solvents such as glycerol.

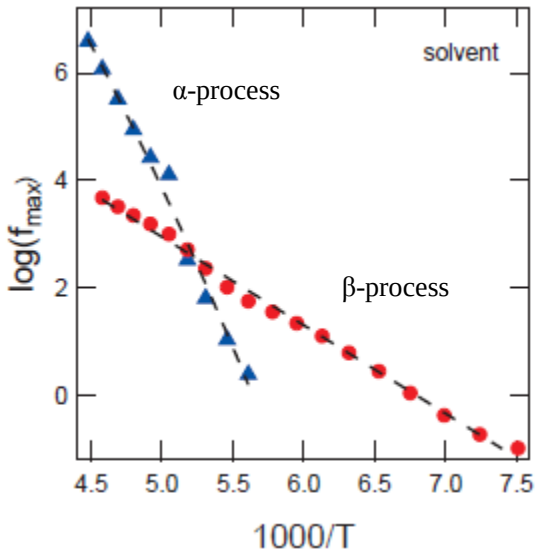

Figure 11: Maximum frequency (f_{max}) as a function of inverse temperature for solvent. The α-relaxation follows a Vogel-Fulcher-Tammann (VFT) behavior whereas the β-relaxation follows an Arrhenius, or linear behavior.

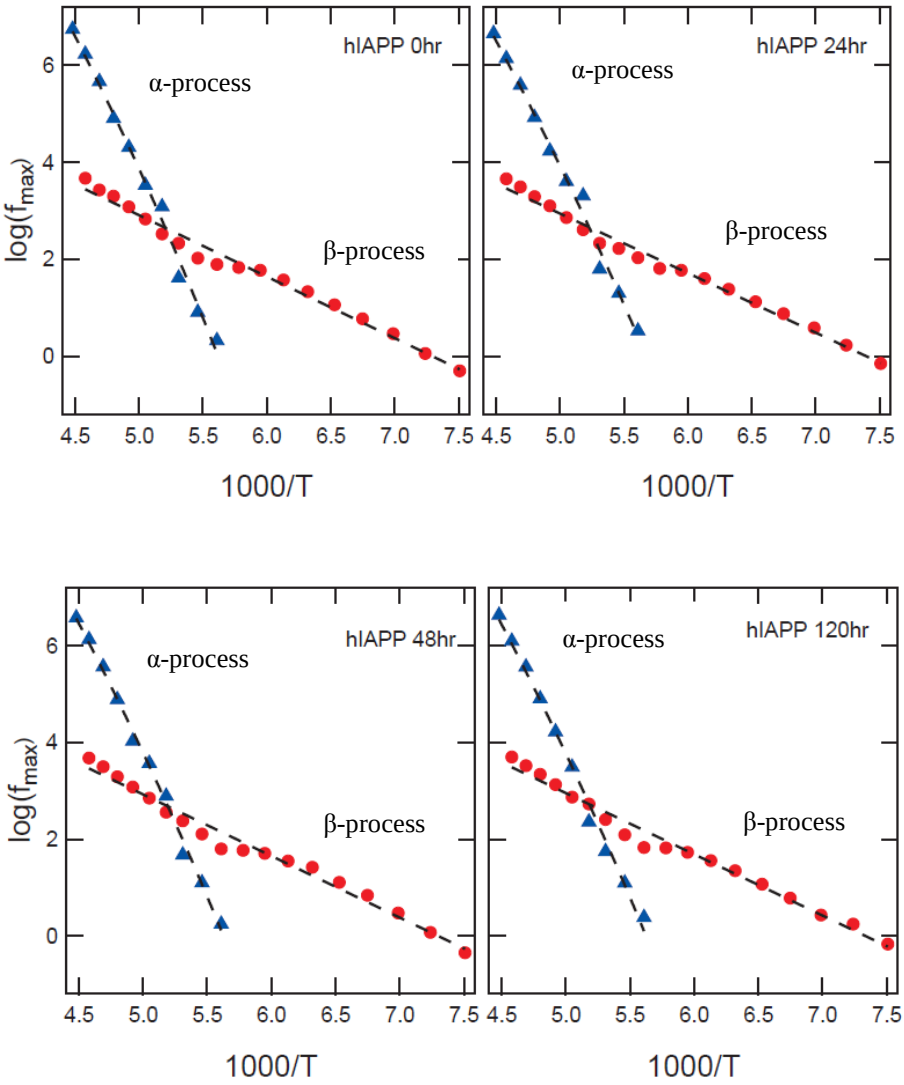

Figure 12: Maximum frequency (f_{max}) as a function of inverse temperature for h-IAPP at incubation time of 0, 24, 48, 120 hours. The α-relaxation follows a Vogel-Fulcher-Tammann (VFT) behavior whereas the β-relaxation follows an Arrhenius, or linear behavior.

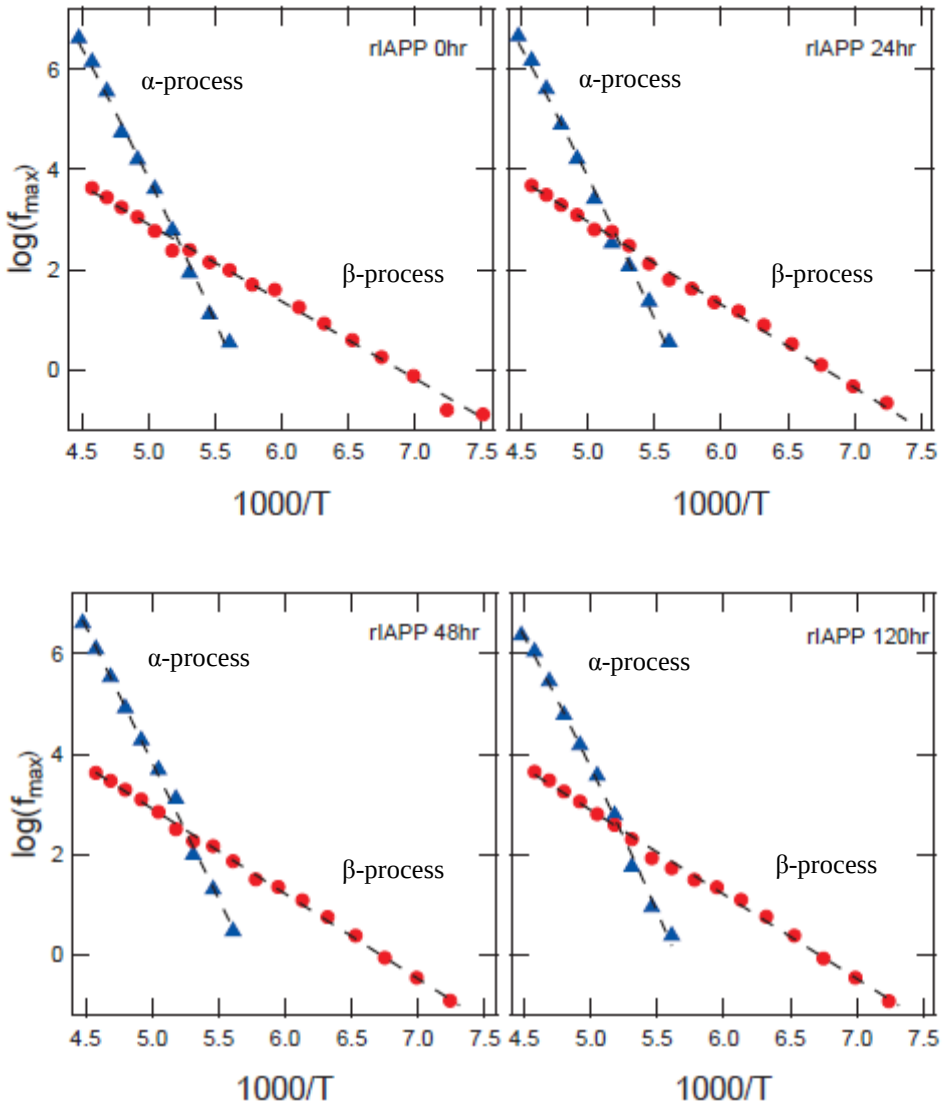

Figure 13: Maximum frequency (f_{max}) as a function of inverse temperature for r-IAPP at incubation time of 0, 24, 48, 120 hours. The α-relaxation follows a Vogel-Fulcher-Tammann (VFT) behavior whereas the β-relaxation follows an Arrhenius, or linear behavior.

3.4.3 Activation Energy

Activation energy is of interest because the changes in the activation energy indicate the changes in hydration water surrounding the amyloidogenic structures. From the slope of the peaks of the β-process, $f_{max} = \frac{1}{2\pi\tau_{max}}$, in Arrhenius plot, activation energy is calculated. The relaxation time follows an Arrhenius type behavior$\tau = \tau_0 e^{-E_a/K_B T}$. The calculated values for activation energies are shown in Table 1 and 2.

Peptide, time	**Activation Energy (E_a) (kJ/mol)**
h-IAPP, 0hr	**24.3**
h-IAPP, 24hr	**23.5**
h-IAPP, 48hr	**24.4**
h-IAPP, 120hr	**24.2**
Solvent	**31.5**

Table 1: Activation energy of solvent and the h-IAPP for incubation times, 0, 24, 48, 120 hours. Different aggregation states are observed by the activation energy. At 0h, the value decreases significantly from its solvent. Overall difference between 0h and 120h is 0.1 kJ/mol. This may be due to a mixture of both parallel and anti-parallel β-sheet conformations dominating at different phases of the aggregation process.

Peptide, time	**Activation Energy (E_a) (kJ/mol)**
r-IAPP, 0hr	**29.5**
r-IAPP, 24hr	**31.7**
r-IAPP, 48hr	**32.4**
r-IAPP, 120hr	**32.2**
solvent	**31.5**

Table 2: Activation energy of solvent and the r-IAPP for incubation times, 0, 24, 48, 120 hours. The value at 0h does decrease as observed in h-IAPP. However, the difference is much smaller. Also, as the time increases, the value increases constantly.

As the proteins aggregates, the water molecules are constantly rearranging and form new hydrogen bonds. In thermodynamics terms, forming a hydrogen bond leads to a decrease in enthalpy (activation energy in our case) which in turns leads to an increase in entropy.

We first compare the protein solution change in the activation energy for the h-IAPP to the activation energy of the solvent. We observe a decrease of the activation energy as compared to solvent at 0h, when the protein is in its monomeric form. As the protein aggregates and water rearranges around the surface of the protein an increase in the activation energy is initially observed and when

fibrils are formed (120h) a decrease in the activation energy follows. This suggest that water molecules form new hydrogen bonding as a result of water liberated in the systems due to fibril formation. For the r-IAPP, at 0h, the value is relatively higher than the value for h-IAPP. Up to 48h, activation energy increases and it even goes higher than the solvent.

3.4.4 Dielectric strength vs. 1000/T

The dielectric strength (Δε) is determined by taking the difference between the static permittivity(ε_s) and the high frequency permittivity(ε_s). And, the relationship of the dielectric strength and the dipole moment is: $\Delta\varepsilon \sim \mu^2$. By looking at the dielectric strength, one may observe stacking structures of proteins. The equation for the dielectric strength is;

$$\boldsymbol{\Delta\varepsilon = \frac{2\varepsilon_0 M k_B T \mu^2}{N_A c g_k}} \qquad (7)$$

where M is the protein molecular mass, ε_0 is the vacuum permittivity, c is the protein concentration in kg/m^3, k_B and N_A are the Boltzmann and Avogadro constants, and g_k denotes the Kirkwood correlation parameter.

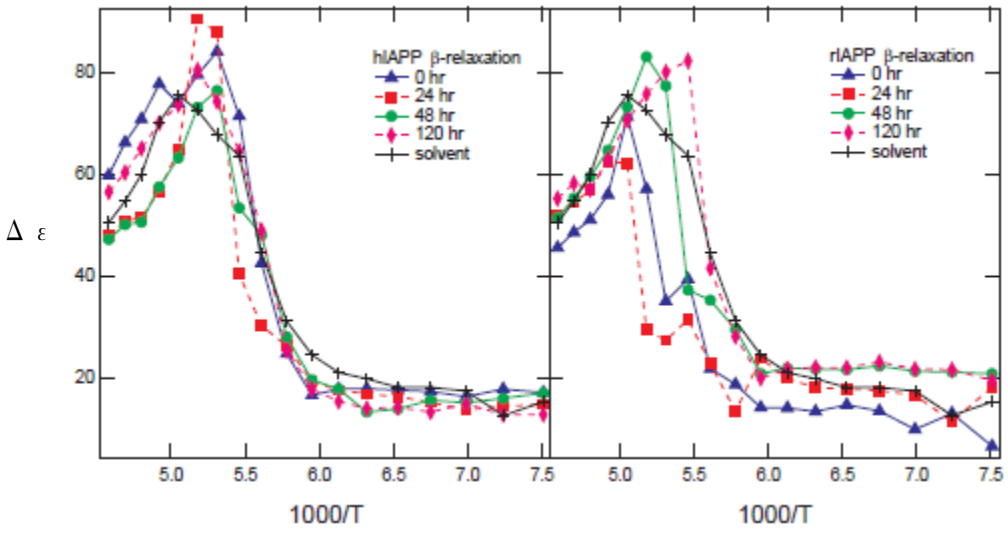

Figure 14: Dielectric strength (Δε) of the β-relaxation for h-IAPP and r-IAPP as a function of inverse temperature. The dielectric strength for the h-IAPP solution first increases, then deceases to values less than the solvent. The dielectric strength of r-IAPP continued to increase over time. This indicates a mixed grouping of parallel and anti-parallel-sheets in hIAPP and random-coil aggregation in rIAPP.

4. Studies of the h-IAPP and the r-IAPP in BSA Buffer

4.1 Overview

In this chapter, dielectric spectroscopy data and analysis is presented for an amyloidogenic peptide and its' non-amyloidogenic analog. Amyloidogenic peptide human islet amyloid polypeptide, h-IAPP (22-27) was used as a model for studying protein aggregation and beta sheet formation in a bovine serum albumin (BSA) buffer. Its' non-amyloidogenic analog, rat islet amyloid polypeptide, r-IAPP (20-29) was selected as a control material. BSA was chosen as a buffer to demonstrate dielectric measurements in the presence of high protein back-ground and to simulate in vivo-like conditions. Trends of dielectric spectra as a function of incubation time and temperature are explored within.

4.2 Sample Preparation

Lyophilized peptides were obtained from AnaSpec, Inc in quantities of 0.5 mg and 1.0 mg. The vials were stored at approximately -20℃ until the time of reconstitution. Bovine serum albumin (BSA) from Sigma was used to dilute and rehydrate the peptides to a concentration of approximately 100μM. The samples were then mixed by repeated inversion of the vials and set to incubate for 0, 8, 24, 48, or 120 hours at room temperature in a 2mL sterile microconical tube. A separate sample was prepared for each time point. Glycerol, 99% minimum from Sigma was then added to a final concentration of 50μM peptide in 50%-50% by weight BSA-glycerol solvent. The samples were

again mixed by repeated inversion of the vials. Each sample was then placed in the Novocontrol BDS 1307 stainless steel sample cell. The measurement was preceded as explained in Ch. 3.3 but here instead of water, BSA was used as the buffer.

4.4 Results and Discussion:

4.4.1 Permittivity vs. Frequency:

Figure 16-19 show permittivity data for h-IAPP and r-IAPP as a function of frequency at different incubation times with the solvent at temperatures 233 K, 223 K, 213 K, 203 K 193 K, 183 K, 173 K, 163 K, and 153K. Some significant differences are shown in these graphs. At 223 K and 213 K, the α-relaxation processes for h-IAPP decreased in magnitude over time. On the other hand, the α-relaxation processes for r-IAPP shifts down first then it comes up back again. At 163 K and 153 K, The β-relaxation process for h-IAPP at 153K trends to higher magnitude over time, while for the process for r-IAPP shifts to a higher magnitude first and comes back to the low magnitude.

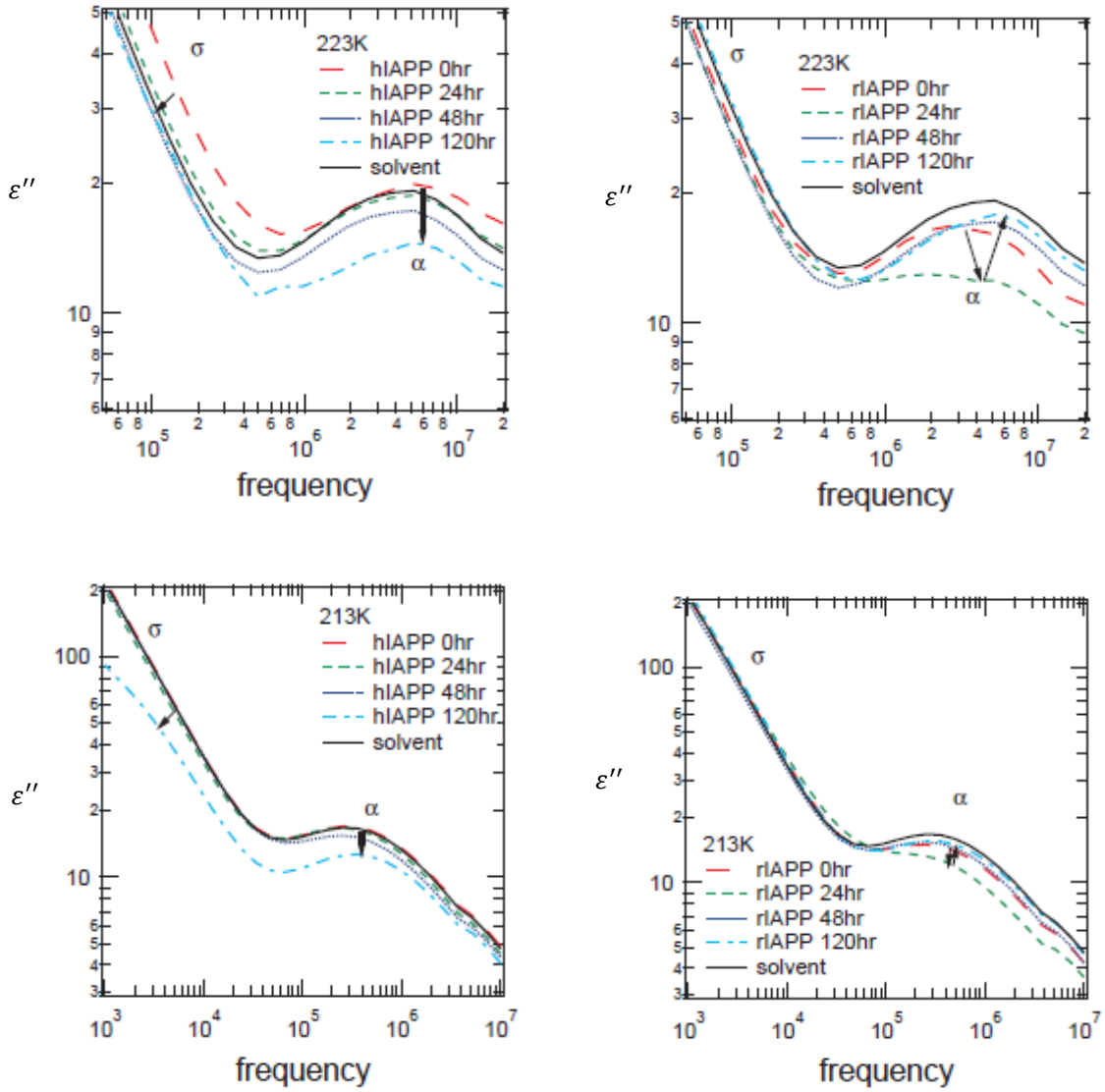

Figure 15: Dielectric loss ε'' as a function of frequency for h-IAPP and r-IAPP at temperatures 223K and 213K and incubation periods of 0, 24, 48, and120 hours. At these temperature range, β-relaxation is dominated my conductivity and is not observed. The α-relaxation processes for h-IAPP decreased in magnitude over time. On the other hand, the α-relaxation processes for r-IAPP shifts down first then it comes up back again.

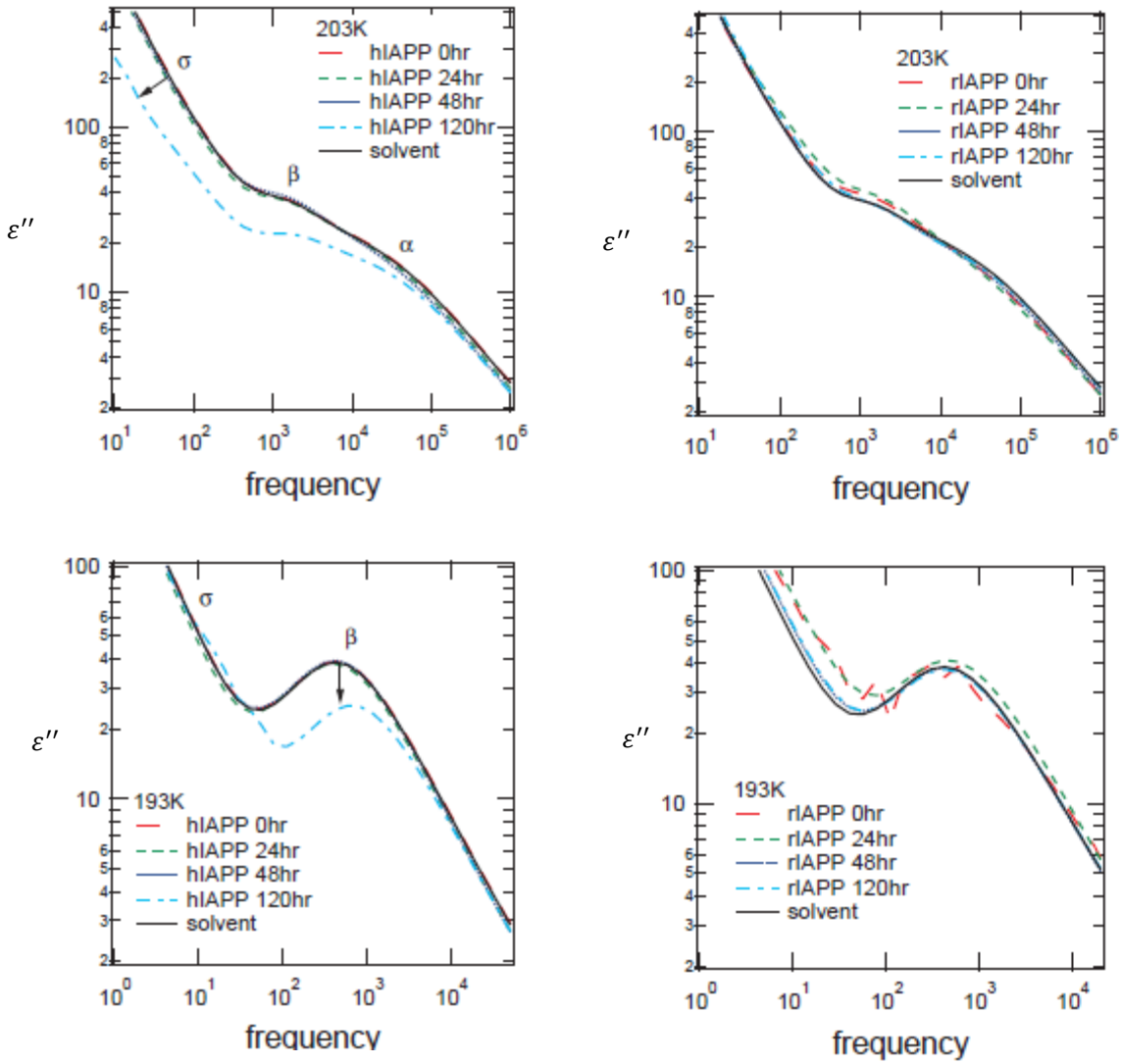

Figure 16: Dielectric loss ε'' as a function of frequency for h-IAPP and r-IAPP at temperatures 203K and 193K and incubation periods of 0, 24, 48, and120 hours. The β-relaxation processes are now shown clearly. The shifts of any of the processes show consistency over time except for the β-process for h-IAPP at 120h; the β-process shifts down.

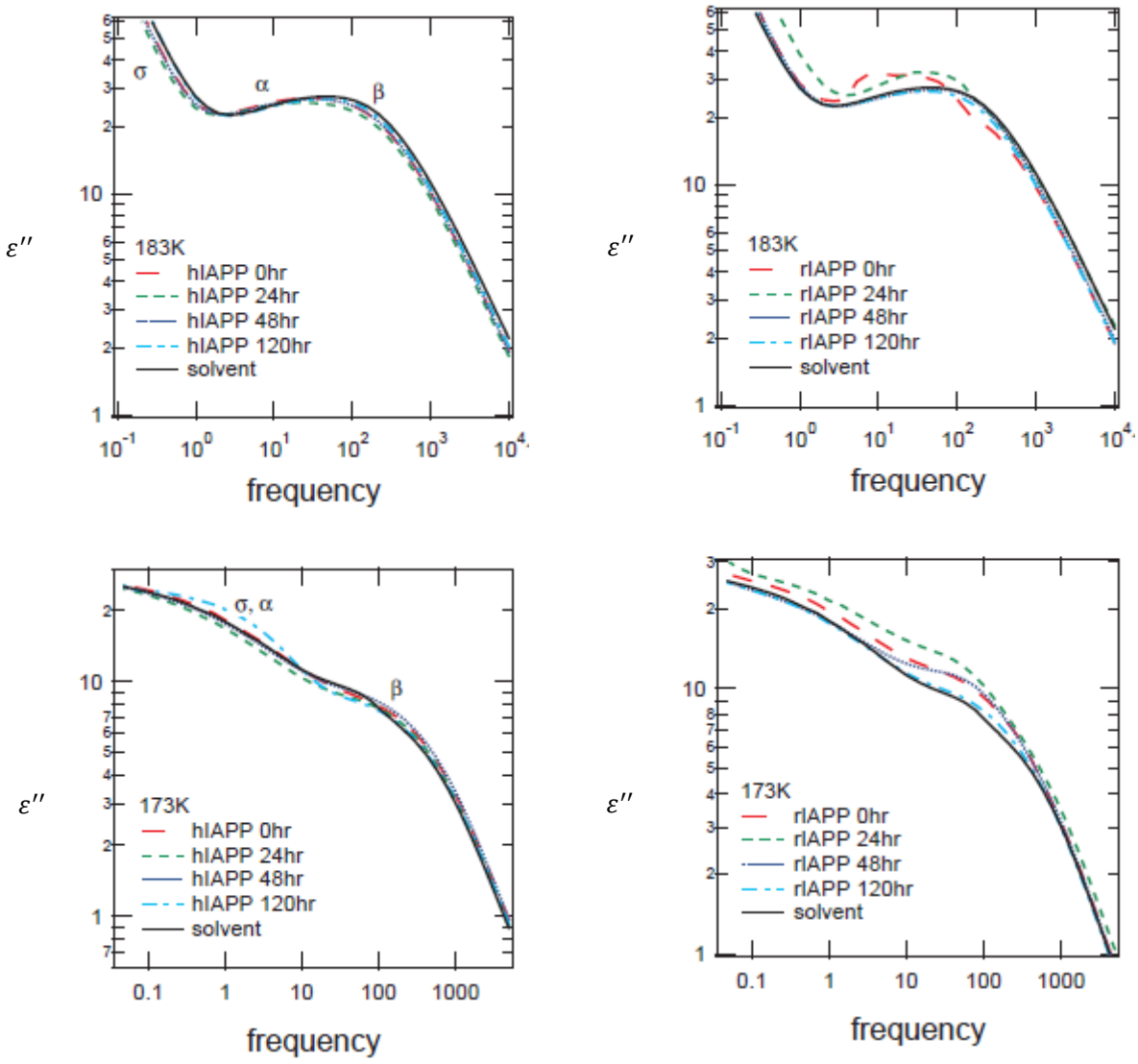

Figure 17: Dielectric loss ε'' as a function of frequency for h-IAPP and r-IAPP at temperatures 183K and 173K and incubation periods of 0, 24, 48, and120 hours. It is hard to determine trends in this range, because the processes are mixed.

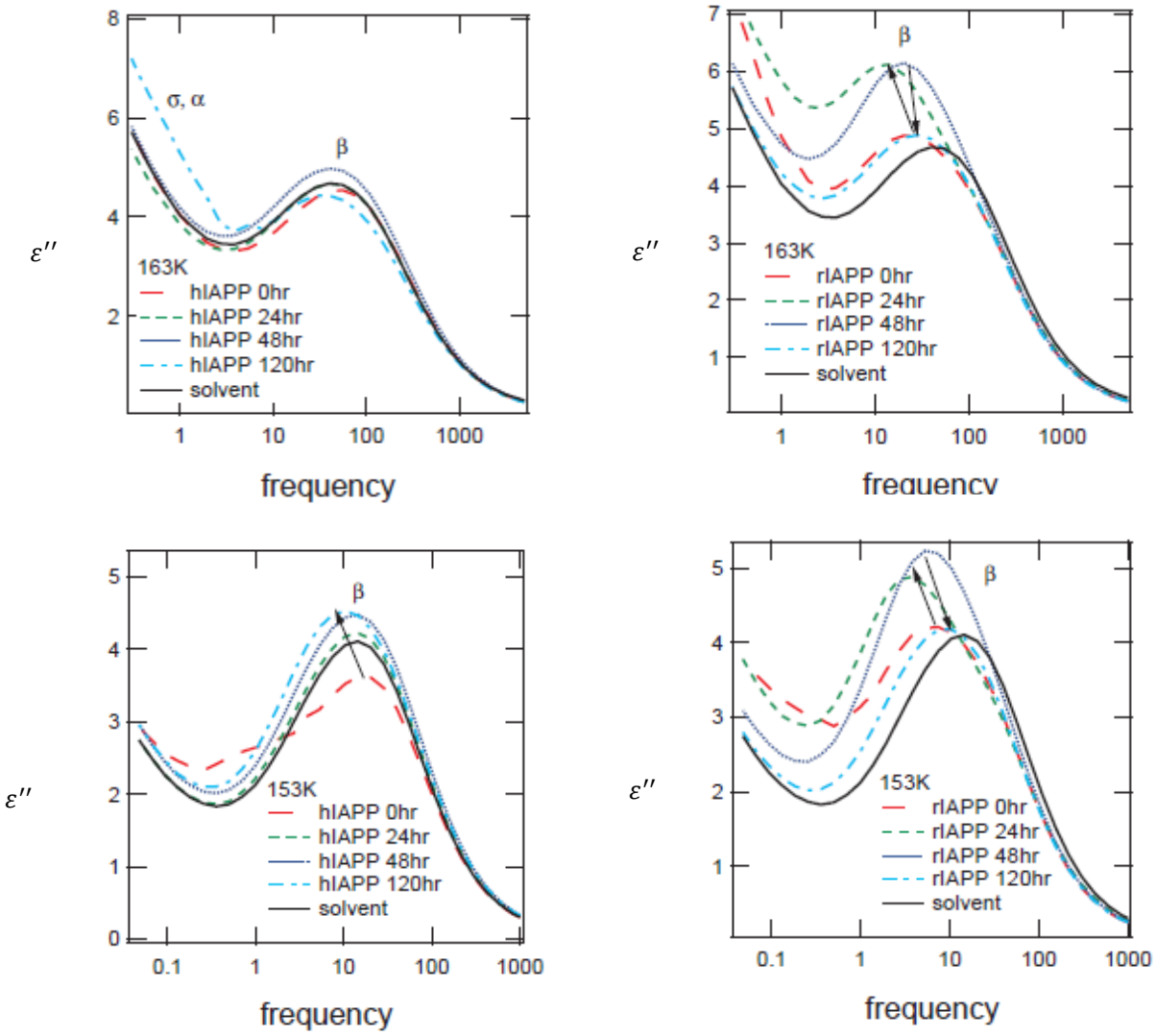

Figure 18: Dielectric loss ε'' as a function of frequency for h-IAPP and r-IAPP at temperatures 163K and 153K and incubation periods of 0, 24, 48, and120 hours. The β-relaxation process for h-IAPP at 153K trends to higher magnitude over time, while for the process for r-IAPP shifts to a higher magnitude first and comes back to the low magnitude.

4.4.2 Relaxation time vs. 1000/T:

By using our fitting functions, the maximum frequency (f_{max}) of the imaginary part of the permittivity of α- and β-relaxation processes were determined. The maximum frequencies were plotted as a function of inverse temperature these are known as Arrhenius plot (Figure 20-22). The β-relaxation process follows a linear, or Arrhenius behavior throughout the temperature range. The α-relaxation process follows a slight non-linear Vogel-Fulcher-Tammann (VFT)-type behavior that is expected in glassforming solvents such as glycerol.

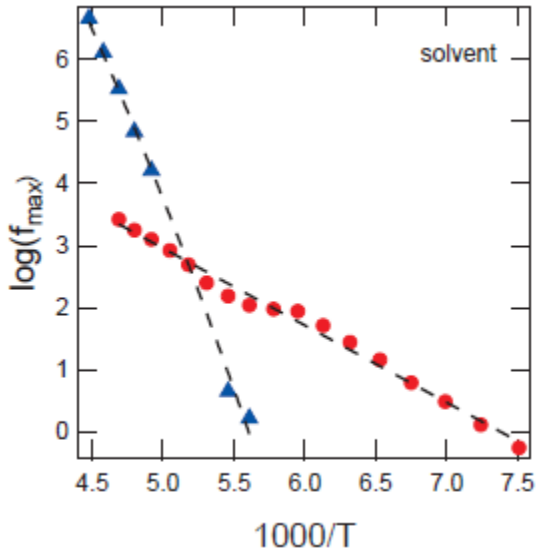

Figure 19: Maximum frequency (f_{max}) as a function of inverse temperature for solvent. The α-relaxation follows a Vogel-Fulcher-Tammann (VFT) behavior whereas the β-relaxation follows an Arrhenius, or linear behavior.

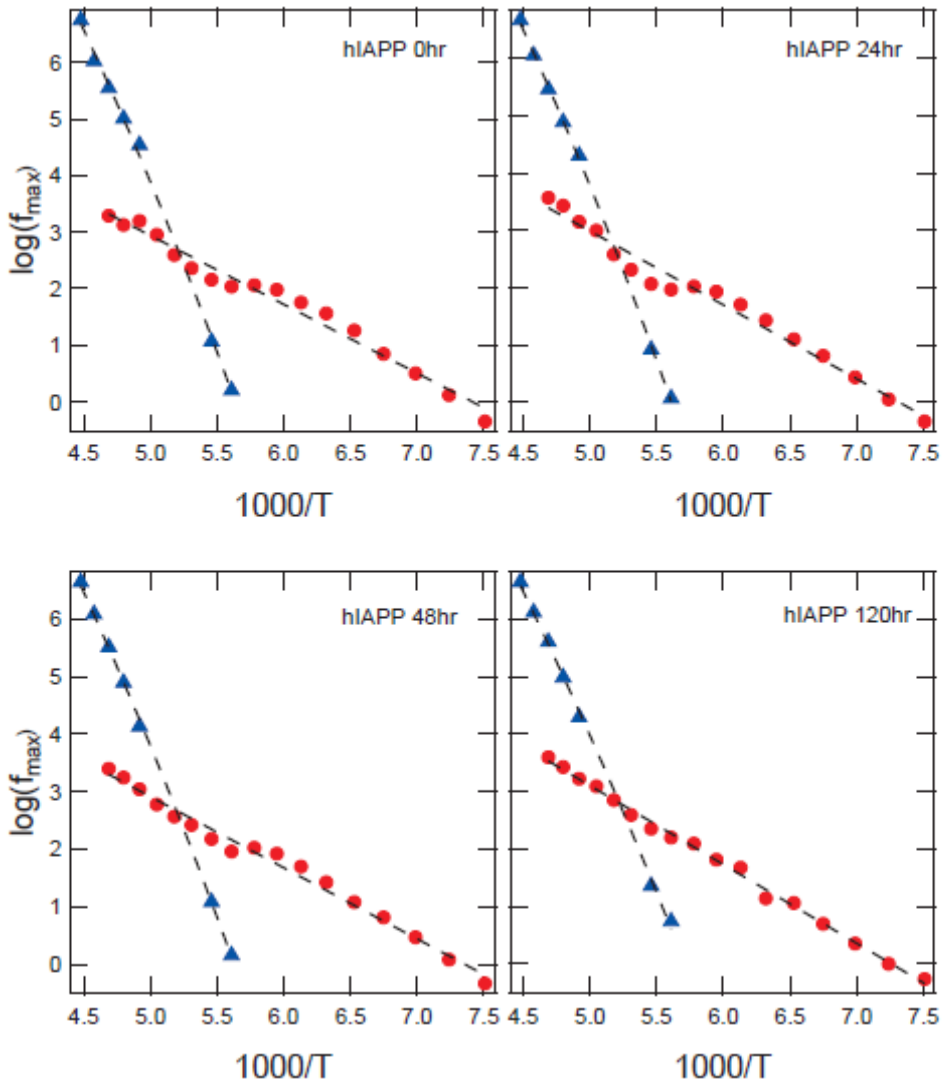

Figure 20: Maximum frequency (f_{max}) as a function of inverse temperature for h-IAPP at incubation time of 0, 24, 48, 120 hours. The α-relaxation follows a Vogel-Fulcher-Tammann (VFT) behavior whereas the β-relaxation follows an Arrhenius, or linear behavior.

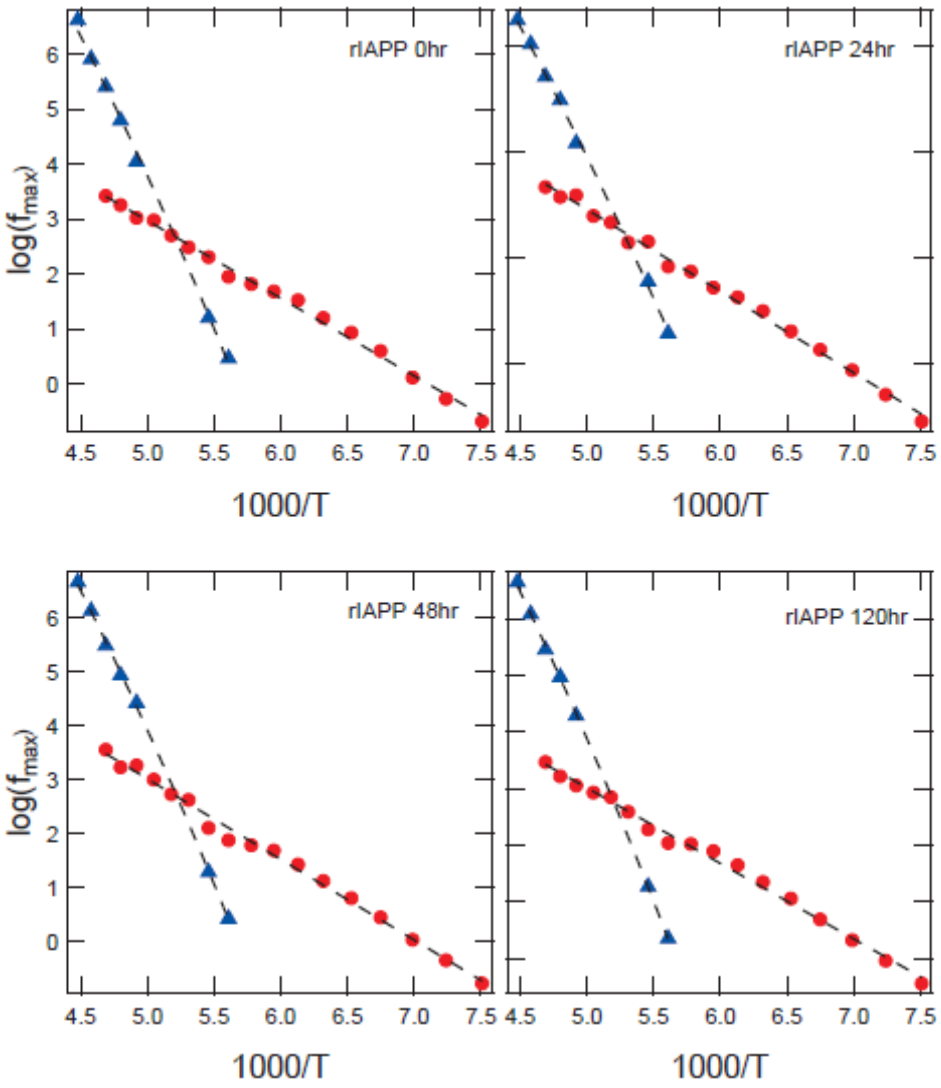

Figure 21: Maximum frequency (f_{max}) as a function of inverse temperature for r-IAPP at incubation time of 0, 24, 48, 120 hours. The α-relaxation follows a Vogel-Fulcher-Tammann (VFT) behavior whereas the β-relaxation follows an Arrhenius, or linear behavior.

4.4.3 Activation Energy

Activation energy is of interest because the changes in the activation energy indicate the changes in hydration water surrounding the amyloidogenic structures. From the slope of the peaks of the β-process, $f_{max} = \frac{1}{2\pi\tau_{max}}$, in Arrhenius plot, activation energy is calculated. The relaxation time follows an Arrhenius type behavior: $\tau = \tau_0 e^{-E_a/K_B T}$. The calculated values for activation energies are shown in Table 3 and 4.

Peptide, time	**Activation Energy (E_a) (kJ/mol)**
h-IAPP, 0hr	**23.3**
h-IAPP, 24hr	**24.7**
h-IAPP, 48hr	**23.7**
h-IAPP, 120hr	**26.3**
solvent	**23.8**

Table 3: Activation energy of solvent and the h-IAPP for incubation times, 0, 24, 48, 120 hours. As seen for the measurement with DI water, the value at 0h is lower than the solvent. At 48h, it decreases due to the mixture of the state but other than that, the value increases constantly.

Peptide, time	**Activation Energy (E_a) (kJ/mol)**
r-IAPP, 0hr	**27.0**
r-IAPP, 24hr	**29.5**
r-IAPP, 48hr	**28.6**
r-IAPP, 120hr	**25.6**
solvent	**23.8**

Table 4: Activation energy of solvent and the r-IAPP for incubation times, 0, 24, 48, 120 hours. Similar to the DI water measurement, the activation energy for the r-IAPP is higher than that of the h-IAPP.

Similar to the result from the DI water measurement, for the h-IAPP we observe a decrease of the activation energy as compared to solvent at 0h, but the value is higher and close to the solvent. As the protein aggregates and water rearranges around the surface of the protein an increase in the activation energy is initially observed. A decrease in the activation energy is shown at 48h and this might be due to the mixture of the aggregation states.

4.4.4 Dielectric strength vs. 1000/T:

Similar to the measurement with DI water, we have determined the dielectric strength to observe the structural information about the proteins using the Eq. 8. Figure 23 shows that over time, h-IAPP displayed a series of increases and decreases in the dielectric strength as fibril formation progresses, with a final dielectric strength much less than the solvent at 120 hours. The non-amyloidogenic r-IAPP did not change over time. The increase and decrease cycles for h-IAPP may be due to a mixture of both parallel and anti-parallel β-sheet conformations dominating at different phases of the aggregation process, but here we see a final state that would appear to be anti-parallel in nature.

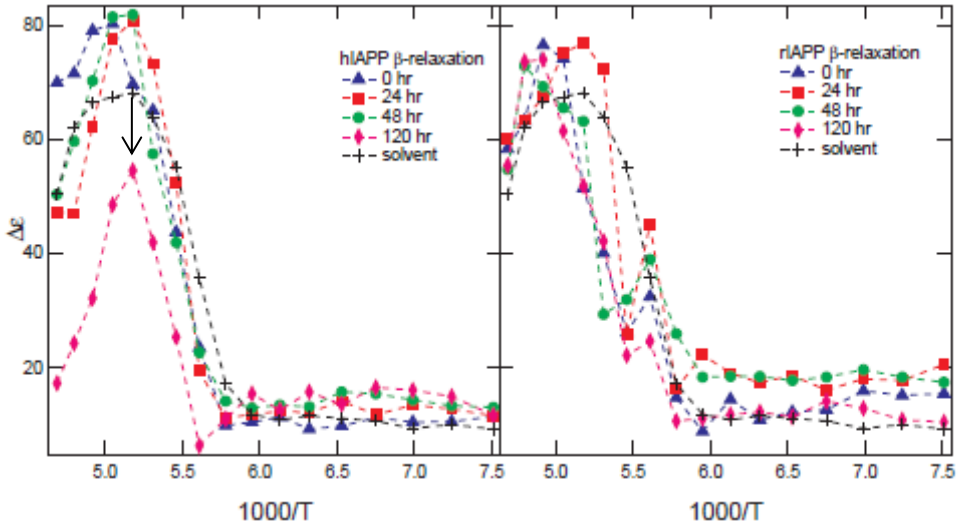

Figure 22: Dielectric strength (Δε) of the β-relaxation for h-IAPP and r-IAPP as a function of inverse temperature. A big drop is observed for the h-IAPP at 120h. This is not seen in the data for r-IAPP. This may be an indication that the final aggregated state of h-IAPP in serum is an antiparallel b-sheet.

4.4.5 Conductivity

Conductivity spectra offer another way to present data for ionically conducting systems. At low frequencies, $\sigma'(\omega)$ is constant at the dc value, $\sigma_0(T)$, which increases only with increasing temperature. At higher frequencies, however, the conductivity increases according to a power law $\sigma'(\omega) \sim \omega^p$ $(0 < p \leq 1)$.[21] The nature of the σ-relaxation, which often is ascribed to the motion of bound water molecules, is not yet fully understood.[22] For sinusoidal electric fields the complex conductivity σ^* and the complex dielectric function ε^* are related by $\sigma^* = iw\varepsilon_0\varepsilon^*$($\varepsilon_0$ being the permittivity of the free space). In figure 23, we present real part of conductivity vs. frequency and in figure 24, Log of the direct current conductivity σ_0 vs. 1000/T.

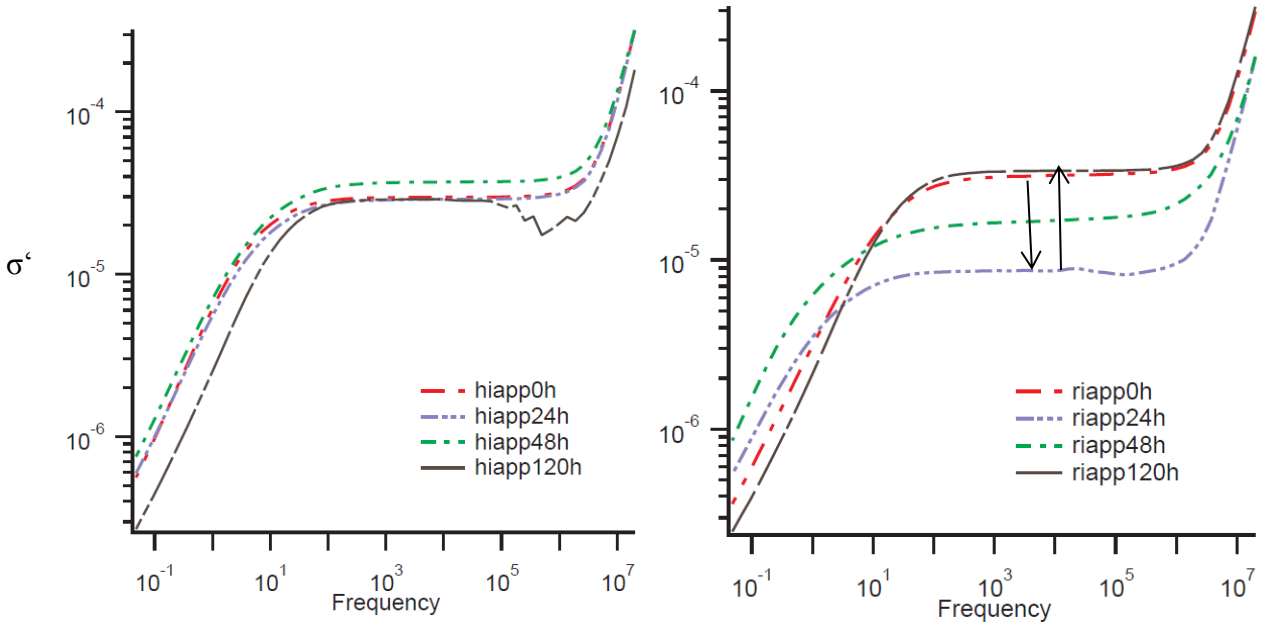

Figure 23 : Real part of conductivity vs. frequency. The h-IAPP does not shift as widely as the r-IAPP does. It is interesting to notice that the changes of the behavior of these seem somehow related to the activation energy. As you can see from the arrows in the r-IAPP, it first shifts down until 48h and it goes back up at 120h. Activation energy showed us the completely opposite behavior. Similar can be said to the h-IAPP.

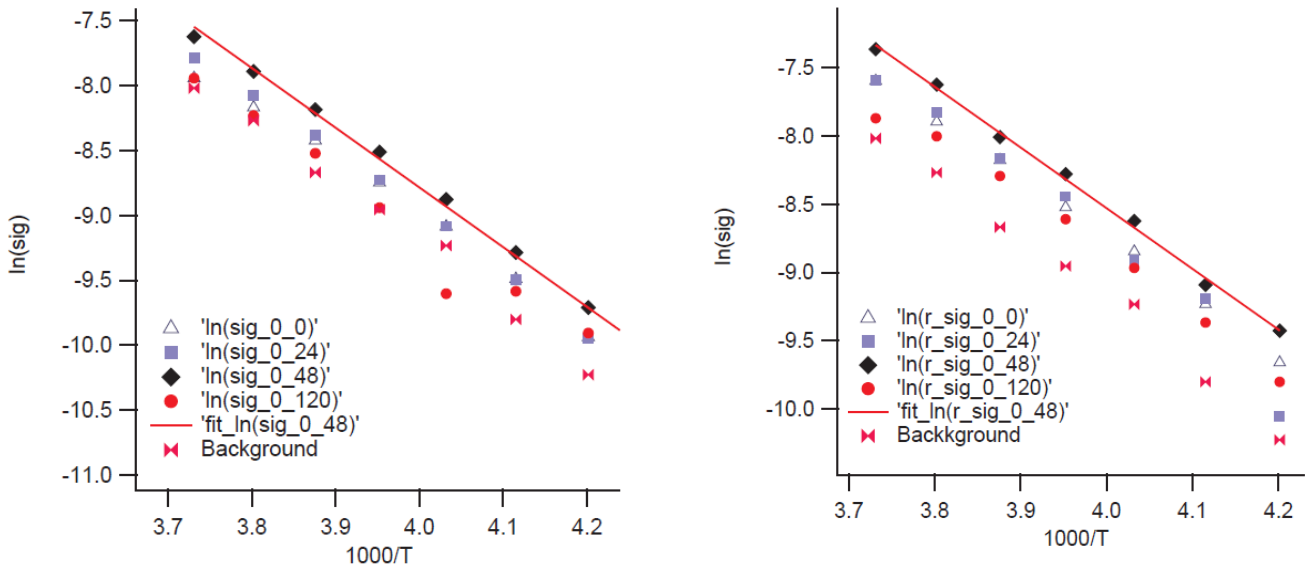

Figure 24: Log of the direct current conductivity σ_0 versus 1000/T for h-IAPP and r-IAPP in the range of temperatures from 273 to 238K at incubation times of 0, 24, 48, 120 hours with their solvent. Overall the conductivity has higher magnitude for the r-IAPP. Both for the h-IAPP and r-IAPP, they have similar trend; the conductivity increases and then decreases.

It seems like that the conductivity is related to the activation energy which tell us that it is related to the structure of the proteins. Conductivity may be a good quantity to further understand the aggregation process and to distinguish between signals given by different molecular species such as monomers, oligomers, protofibrils and fibrils. However more work should be done in future.

5. Conclusion

We have demonstrated the dielectric response of h-IAPP (22-27) and r-IAPP (20-29) in the presence of a deionized water-glycerol solvent and BSA-glycerol solvent. The spectra disclose that the amyloidogenic peptide can be detected and differentiated from its non-amyloidogenic analogs using dielectric relaxation spectroscopy. We have analyzed at the data in the following ways: Permittivity vs. Frequency, Relaxation time vs. 1000/T, Activation Energy, Dielectric strength vs. 1000/T.

Our results indicate that DRS is a sensitive measurement technique for determining the changes in the hydration water of different amyloidogenic molecular structures and therefore for detecting amyloidogenic precursors.

[1] Claudio Soto. Protein misfolding and disease; protein refolding and therapy. FEBS Letters, 498(2-3):204-207, 2001. Lisbon Special Issue.

[2] Christopher M. Dobson. The structural basis of protein folding and its links with human disease. Philosophical Transactions of the Royal Society of London. Series B: Biological Sciences, 356(1406):133-145, 2001.

[3] Center for Disease Control and Prevention. 2011 national diabetes fact sheet. 2011.

[4] P Westermark, C Wernstedt, E Wilander, D W Hayden, T D O'Brien, and K H Johnson. Amyloid fibrils in human insulinoma and islets of langerhans of the diabetic cat are derived from a neuropeptide-like protein also present in normal islet cells. Proceedings of the National Academy of Sciences, 84(11):3881-3885,1987.

[5] A. Lorenzo and B. A. Yankner. Amyloid fibril toxicity in Alzheimer's disease and diabetes. Annals of the New York Academy of Sciences, 777(1):89-95, 1996.

[6] P Westermark, U Engstrom, K H Johnson, G T Westermark, and C Betsholtz. Islet amyloid polypeptide: pinpointing amino acid residues linked to amyloid fibril formation. Proceedings of the National Academy of Sciences, 87(13):5036-5040, 1990.

[7] A. Clark, M.R. Nilson, Islet amyloid: a complication of islet dysfunction or an aetiological factor in Type 2 diabetes?, Diabetologia (2004) 47: 157-169

[8] Magdalena Anguiano, Richard J. Nowak, and Peter T. Lansbury. Protofibrillar islet amyloid

polypeptide permeabilizes synthetic vesicles by a pore-like mechanism that may be relevant to type II diabetes. Biochemistry, 41(38):11338-11343, 2002. PMID: 12234175.

[9] Tajib A. Mirzabekov, Meng-chin Lin, and Bruce L. Kagan. Pore formation by the cytotoxic islet amyloid peptide amylin. Journal of Biological Chemistry, 271(4):1988-1992, 1996.

[10] Steven E. Kahn. The importance of beta-cell failure in the development and progression of type 2 diabetes. Journal of Clinical Endocrinology & Metabolism, 86(9):4047-4058, 2001.

[11] J.M. Berg, J.L. Tymoczko, and L. Stryer. Biochemistry. W. H. Freeman, 2006.

[12] Hans Frauenfelder, Guo Chen, Joel Berendzen, Paul W. Fenimore, Helen Jansson, Benjamin H. McMahon, Izabela R. Stroe, Jan Swenson, and Robert D. Young. A united model of protein dynamics. Proceedings of the National Academy of Sciences, pages 1-6, 2009.

[13] Yuri Feldman, Alexander Puzenko, and Yaroslav Ryabov. Dielectric Relaxation Phenomena in Complex Materials, pages 1-125. John Wiley & Sons, Inc., 2005.

[14] A. Serghei, M. Tress, J. R. Sangoro, and F. Kremer. Electrode polarization and charge transport at solid interfaces. Phys. Rev. B, 80:184301, Nov 2009.

[15] J. L. Oncley. Studies of the dielectric properties of protein solutions. i. carboxyhemoglobin1,2. Journal of the American Chemical Society, 60(5):1115-1123,1938.

[16] J. L. Oncley. The investigation of proteins by dielectric measurements. Chemical Reviews, 30(3):433-450, 1942.

[17] Y. Hayashi, A. Guitina, and Y. Feldman. Low frequency liquid sample holder: Three electrode type. Dielectrics Newsletter, (21):6-7, 2005.

[18] Florin Despa, Ariel Fernandez, L.Ridgway Scott, and R.Stephen Berry. Hydration profiles of amyloidogenic molecular structures. Journal of Biological Physics, 34:577-590, 2008.

[19] Ariel Fernndez, Jozsef Kardos, L. Ridgway Scott, Yuji Goto, and R. Stephen Berry. Structural defects and the diagnosis of amyloidogenic propensity. Pro-ceedings of the National Academy of Sciences, 100(11):6446-6451, 2003.

[20] Florin Despa, Ariel Fernandez, L.Ridgway Scott, and R.Stephen Berry. Hydration profiles of amyloidogenic molecular structures. Journal of Biological Physics, 34:577-590, 2008.

[21] Mingyun Sun, Srdjan Pejanovic, and Jovan Mijovic. Dynamics of Deoxyribonucleic Acid Solutions As Studied by Dielectric Relaxation Spectroscopy and Dynamic Mechanical Spectroscopy 38, 9854-9864 September 16, 2005

[22] M. Wolf, R. Gulich, P. Lunkenheimer, A. Loidl. Relaxation dynamics of a protein solution investigated by dielectric spectroscopy. Biochim. Biophys. Acta. 1824,723 February 15, 2012